Surface and interface topography of amorphous SiO_2/crystalline Si(100) studied by X-ray diffraction

1990 J. Phys.: Condens. Matter 2 8869

(http://iopscience.iop.org/0953-8984/2/45/003)

J. Phys.: Condens. Matter **2** (1990) 8869–8879. Printed in the UK

Surface and interface topography of amorphous SiO_2/ crystalline Si(100) studied by x-ray diffraction

L Brügemann†, R Bloch†, W Press† and P Gerlach‡

† Institut für Experimentalphysik, Universität Kiel, Leibnizstraße 19, D-2300 Kiel 1, Federal Republic of Germany

‡ Wacker Chemitronic, Postfach 1140, D-8263 Burghausen, Federal Republic of Germany

Received 3 April 1990

Abstract. Several samples of a-SiO_2/c-Si(100) with different oxide layer thicknesses and different silicon surface qualities were examined by x-ray diffraction. The layer thickness as well as the surface roughness and the interface roughness were studied by measuring the reflectivity of the samples near total external reflection. A separate and detailed determination of the interface roughness is obtained by analysing the intensity near the Si(400) reciprocal lattice point. There is a pronounced diffuse scattering parallel to the normal of the interface, the frequently called crystal truncation rods. Both the reflectivity and the isointensity contours around the (400) reflection demonstrate the presence of an intermediate layer between a-SiO_2 and c-Si in a crystalline state.

1. Introduction

The quality of the surface and the interface of the system SiO_2 on Si(100) is of great interest in both semiconductor technology and physical sciences. Transmission electron microscopy investigations [1, 2] show that a crystalline SiO_2 (c-SiO_2) layer exists at the amorphous SiO_2 (a-SiO_2)–crystalline Si(100) (c-Si(100)) interface. This is confirmed for example by core-level spectroscopy [3] and x-ray scattering studies [4]. In particular the roughness of the interface between Si(111) and thin oxide layers were studied by x-ray scattering [5].

Two complementary techniques of x-ray scattering are used in the present study to evaluate the roughness of the surface, the thickness of the oxide layer and the roughness of the interface.

(a) Reflectivity measurements near the angle of total external reflection show interference maxima related to the layer thickness [6]. The decrease in the reflected intensity is also influenced by the roughness of the surface [6–8].

(b) The lattice periodicity is terminated by the surface abruptly. This gives rise to scattering of x-rays with momentum transfer parallel to the normal of the surface. The decrease in the intensity along the so-called crystal truncation rods (CTRs) [9] depends

0953-8984/90/458869 + 11 $03.50

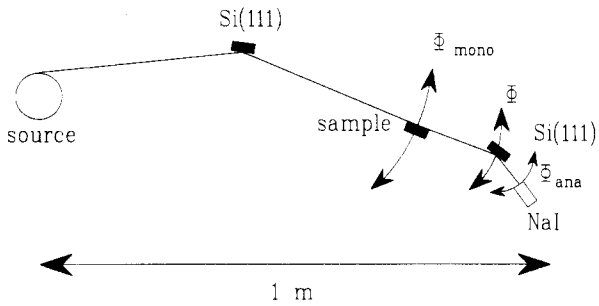

Figure 1. A schematic diagram of the TCD.

on the roughness of the crystalline surface and on the density profile parallel to the surface normal.

2. The experiment

Both the reflectivity of the samples and the intensity distribution around the (400) reciprocal lattice point of silicon were measured with a triple crystal diffractometer (TCD) [10] (figure 1). The x-ray source was a 12 kW rotating-anode generator (Rigaku RU200) with a magnetically sealed copper target. Two slits in front of the perfect, symmetrically cut Si(111) monochromator and in front of the sample ensure that only Cu $K\alpha_1$ radiation ($\lambda = 1.540\,56$ Å) is incident on the sample. A second identical Si(111) analyser crystal and a NaI(Tl) scintillation counter were used as a detection unit.

The advantage of the TCD technique in comparison with the conventionally used double-crystal diffractometer technique is founded on the angular collimation by Bragg reflection of the scattered radiation by the analyser crystal. This results in very good resolution even though the distance between sample and analyser is 0.3 m and this is rather small. Another great advantage is the high signal-to-background ratio. Modifications of the intensity due to undulations of the surface are largely avoided, an aspect which is very important when measuring the reflectivity of a sample at angles near total external reflection.

The resolution of the TCD used was calculated following the treatment of Cowley [11] and measured near several reciprocal lattice points [12]. The experimentally determined values are 4×10^{-4} Å^{-1} parallel to and 2×10^{-6} Å^{-1} perpendicular to the scattering vector for $|\boldsymbol{Q}| = 0.05$ Å^{-1} and 9×10^{-4} Å^{-1} and 1.3×10^{-4} Å^{-1} for $|\boldsymbol{Q}| = 4.63$ Å^{-1} (Si(400) reflection). These are in agreement with the calculated values.

The TCD technique is well suited to measuring isointensity contours near a reciprocal lattice point, especially the intensity profile of the CTR [9, 13]. The rod profile can be obtained by scanning the scattering vector $\boldsymbol{Q}$ along the direction [011] perpendicular through the rod as a function of $|\boldsymbol{Q}|$ offset q_{pl} along the [100] direction. The accompanying diffuse scattering can simply be subtracted [14].

The samples were prepared from highly polished Si(100) wafers 0.1 m in diameter supplied by Wacker Chemitronic, Burghausen, Federal Republic of Germany. One half of each wafer had been oxidized several times. After every step of oxidation the oxide layer was removed by etching the sample in hydrofluoric acid (HF). After this procedure the silicon surface possesses a higher roughness. The sectional area of an incident laser beam is expanded through the reflection on the surfaces of the etched samples. Finally oxide layers with a well defined thickness were produced by heating the samples to 1000 °C in an Ar atmosphere. Then a small amount of oxygen was added to the argon.

We measured three pairs of samples prepared in this way. The nominal thicknesses, determined by diffraction of visible light are 1420 Å for samples A_s and A_r, 257 Å for B_r, 268 Å for B_s, 222 Å for C_r and 239 Å for C_s. The index r denotes that part of each wafer that has passed through the above treatment (and hence is expected to be rough); the index s denotes the part of the wafer with a smooth surface (not etched).

3. Theory

The calculation of the x-ray reflection curves follows the treatment of Parratt [6], who applied Maxwell's theory to layered systems. The scattering plane is chosen as the x–z plane with the z axis pointing into the medium, parallel to the surface normal. The electric field vectors in the mth layer of the impinging plane electromagnetic wave and of the reflected wave, denoted by $\boldsymbol{E}_m$ and $\boldsymbol{E}_m^{\mathrm{R}}$, respectively, are given by

$$\boldsymbol{E}_m(z) = \boldsymbol{E}_m(0)\exp\{\mathrm{i}[\omega t - (\boldsymbol{k}_{m,x}\cdot\boldsymbol{x} + \boldsymbol{k}_{m,z}\cdot z)]\} \tag{1a}$$

and

$$\boldsymbol{E}_m^{\mathrm{R}}(z) = \boldsymbol{E}_m^{\mathrm{R}}(0)\exp\{\mathrm{i}[\omega t - (\boldsymbol{k}_{m,x}\cdot\boldsymbol{x} - \boldsymbol{k}_{m,z}\cdot z)]\}. \tag{1b}$$

The magnitude of the wavevector $\boldsymbol{k}_m$ in the layer m with the refractive index n_m is given by

$$k_m = 2\pi n_m/\lambda. \tag{2}$$

For x-rays the refractive index n is given by $n = 1 - \delta - \mathrm{i}\beta$ with the optical constants $\delta = \lambda^2 r_e\rho/2\pi$ and $\beta = \lambda\mu/4\pi$. In these two equations, r_e is the classical electron radius, ρ is the electron density and μ is the linear absorption coefficient. As the real parts of the refractive indices are slightly below unity, total reflection of the x-rays occurs for incident angles smaller than 0.5°.

A mathematically applicable recursion expression is obtained from equation (1) if the boundary conditions for the tangential components of the magnetic and electric field are taken into account [10]:

$$F_{m-1}(d_{m-1}) = \frac{(f_{m-1} - f_m) + (f_{m-1} + f_m)F_m(d_m)\exp(-2\mathrm{i}k_0 f_m d_m)}{(f_{m-1} + f_m) + (f_{m-1} - f_m)F_m(d_m)\exp(-2\mathrm{i}k_0 f_m d_m)} \tag{3}$$

with $F_m(z) = E_m^{\mathrm{R}}(z)/E_m(z)$ and $f_m = n_m\sin\theta_m$. The reflectivity as a function of the incident angle θ yields

$$R(\theta) = |F_0|^2 = |E_0^{\mathrm{R}}/E_0|^2. \tag{4}$$

As done by several workers [10, 13] the surface roughness can be considered as a static Debye–Waller factor (DWF) given by

$$\mathrm{DWF} = \exp(-\Delta z^2 k^2\sin^2\theta) \tag{5}$$

with the roughness parameter $\Delta z^2 = \langle h^2(x, y)\rangle$. $h(x, y)$ is a random distribution function which describes the variation in the height h of the surface around its mean height $\langle h\rangle$. In general a height–height correlation function has to be considered but for most cases a gaussian correlation can be used and equation (5) is applicable [15].

An alternative description of the surface or interface roughness was given by Wu and Webb [8]. They introduced a transition layer of thickness T between two media with refractive indices n_1 and n_2, where the refractive index varies as

$$n = \tfrac{1}{2}(n_1 + n_2) + \tfrac{1}{2}(n_1 - n_2)\tanh(-\pi + 2\pi z/T) \qquad z \in [0, T]. \tag{6}$$

To calculate the reflection curves, the transition layer is subdivided into 20 layers of equal thickness t. This method leads to the same results as the introduction of the DWF if the phase differences $\Delta\varphi$ of the waves, which are scattered from neighbouring planes, are small ($\Delta\varphi \ll \pi$) [16]. A great advantage of an approach based on the solution of the wave equation is the possibility of introducing different profiles for the transition layer [17].

The reflectivity $R(\theta)$ is calculated from equation (3) either by including equation (5) or with 20 additional sublayers with refractive indices given by equation (6); reflections from the back side of the substrate are excluded.

For the second type of investigation the theory of CTRs formulated by both Robinson [9] and Andrews and Cowley [13] is applied. Although scattering between the reciprocal lattice points is due to the sharp boundaries of the crystal (especially the abrupt termination of the lattice at the surface), a kinematical approach can be used [9]. This is correct because the surface scattering is weak and multiple-scattering effects can be neglected. Furthermore only the intensity decrease of the CTRs far away from a reciprocal lattice point is interesting. For a perfectly cut surface an intensity decrease

$$I(q) \sim q_{\mathrm{pl}}^{-2} \tag{7}$$

is obtained [9], where q_{pl} is the component of the difference $Q - Q_{(400)}$ along [100]. The same intensity decrease is obtained from the dynamical theory of x-ray diffraction [18, 19]. Two models describing the surface roughness are used.

(1) Comparable with the analysis of the reflection measurements a gaussian roughness can be introduced by a DWF

$$I \sim q_{\mathrm{pl}}^{-2} \exp[-\tfrac{1}{2}(q_{\mathrm{pl}}\,\Delta z)^2]. \tag{8}$$

(2) Most of the measurements have shown that the intensity of the CTR decays with an exponent r with $2 \leqslant r < 4$ [9], which provides an alternative description:

$$I \sim q_{\mathrm{pl}}^{-r}. \tag{9}$$

This exponent r can be related to the fractal dimensions of a rough surface [5, 20].

Both models have been fitted to our data. The parameters Δz^2 and r are determined by means of a least-squares refinement.

4. Results and discussion

In order to determine the density profile and the surface roughness we measured the reflectivity of samples A_r, A_s, B_r and B_s up to a scattering vector $|\boldsymbol{Q}|$ of 0.17 Å^{-1} (samples C_r and C_s were not studied, because the thicknesses of their oxide layers are nearly the

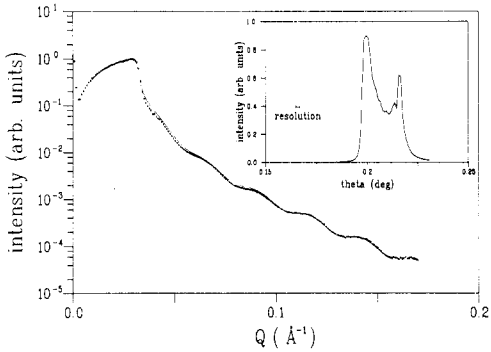

Figure 2. Reflectivity of sample A_s: calculation with a gaussian roughness (——) and measurement (. . . . .). The inset shows a rocking curve for a scattering angle Φ of 0.4°.

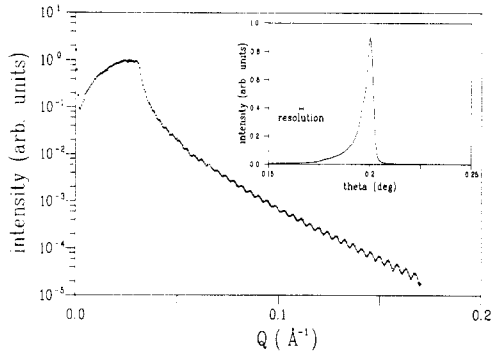

Figure 3. Reflectivity of sample B_s: calculation with a gaussian roughness (——) and measurement (. . . . .). The inset shows a rocking curve for a scattering angle Φ of 0.4°.

same as those of samples B_r and B_s). Figures 2 and 3 show the $|\boldsymbol{Q}|$-dependent intensities from samples A_s and B_s on a logarithmic scale outside the medium (dotted curves) together with the results of the least squares fits (full curves). The background has been subtracted.

Near $|\boldsymbol{Q}| = 0$ Å^{-1} the reflectivity curves show the part of the incident beam which is not masked by the sample. Then a sinusoidal increase in the reflected intensity is observed; the effect is purely geometrical and is related to the part of the incident beam 'seen' by the sample and undergoing total external reflection. For $|\boldsymbol{Q}| = 0.0323$ Å^{-1} the critical angle θ_c of total external reflection is reached and the intensity decreases rapidly. For still increasing $|\boldsymbol{Q}|$-values, interferences between waves reflected from the top and the bottom of the SiO_2 layer become observable, the so-called Kiessig [21] fringes.

The insets in figures 2 and 3 show measurements during which the sample is rotated for a fixed scattering angle Φ of 0.4° (rocking curve). The shape of the curves indicates the macroscopic departure from flatness of the surface of the samples on a micrometre length scale. Great departures from flatness yield very broad rocking curves and seriously degrade the resolution of conventional reflectivity measurements. Moreover the above-described theory for x-ray reflectivity measurements is not able to consider these departures from flatness, but the rocking curves of the samples examined here are much narrower than θ_c so that no influence of the surface undulations on the measured intensities is expected. The rocking curves of the etched samples show a FWHM which is nearly twice as broad as the FWHM of the untreated samples. This is due to long-wavelength undulations of the surface which give rise to a divergent reflected beam.

The following fitting parameters are used: the thickness of the oxide layer, the decrement δ of the refractive index of the layer and the roughness parameter Δz^2 or, equivalently, the thickness T of a transition layer. The results for the samples A_r, A_s, B_r and B_s are listed in table 1. The χ^2-values are calculated with the assumption of an intensity error of 5% for all $|\boldsymbol{Q}|$-values. This is considerably more than the true error and leads to a constant estimation of all data points. Figures 2 and 3 show the calculated intensity for the model using a gaussian roughness of the surface. The results are virtually identical to those based on the model with a transition layer between SiO_2 and vacuum. The assumption of a second transition layer or an interfacial roughness between c-Si and

Table 1. Results of least-squares fits to the data of samples A_r, A_s, B_r and B_s. The surface roughness is described by two models: the first is by a static DWF with Δz^2 and the second is by a tanh-like transition layer to the vacuum of thickness T. d_n is the nominal oxide layer thickness, d_1 is the thickness of the oxide layer considering a DWF (first model), d_{11} is the thickness of a transition layer (second model) and d_2 is the thickness of the intermediate layer. The χ^2-values are calculated by assuming a 5% error for each data point (see text).

Parameter (units)		Value for the following samples			
		A_r	A_s	B_r	B_s
d_n	(Å)	1420	1420	257	268
$\sqrt{\Delta z^2}$	(Å)	7.0 ± 0.5	5.7 ± 0.7	7.1 ± 0.1	7.8 ± 0.1
T	(Å)	48 ± 1	40 ± 1	51 ± 1	59 ± 1
d_1	(Å)	225 ± 3	224 ± 1	1397 ± 1	1410 ± 1
d_{11}	(Å)	201 ± 2	204 ± 1	1375 ± 1	1383 ± 1
δ_1	(10^{-6})	7.44 ± 0.04	7.38 ± 0.02	7.1 ± 0.03	7.21 ± 0.03
d_2	(Å)	17 ± 7	25 ± 2	—	—
δ_2	(10^{-6})	7.91 ± 0.02	7.78 ± 0.02	—	—
ρ	(g cm^{-3})	2.27	2.26	2.19	2.24
χ^2		0.28	0.2	0.46	0.59

a-SiO_2 does not lead to better agreement between the measurements and the model calculation.

All determined oxide thicknesses are slightly smaller than the nominal thicknesses obtained from light diffraction. The higher precision of the reflection measurement is not unexpected; the refractive index can be refined from experimentally determined intensities (depends essentially on θ_c) which is not possible with light scattering. Furthermore the number of interference maxima is greater in the x-ray experiments.

For SiO_2 the decrement δ of the refractive index for x-rays is between 7.44×10^{-6} and 7.1×10^{-6}, while $\delta = 7.55 \times 10^{-6}$ for c-Si [22]. From equation (10) [5, 7] it is possible to estimate the density of the a-SiO_2 layer:

$$\delta \simeq \tfrac{1}{2}(1.64 \times 10^{-3}\lambda\rho^{1/2})^2. \tag{10}$$

The four samples A_r, A_s, B_r and B_s show densities which are 2.5–6% (table 1) smaller than that of c-Si. These differences are very close to those given by Weast [23]: $\rho = 2.3296$ g cm^{-3} for c-Si and $\rho = 2.19$ g cm^{-3} for a-SiO_2. The densities are slightly higher than those given by Cowley and Ryan [5]. It should be noted, however, that their oxide layers were prepared on a different surface orientation (Si(111)).

For samples B_r and B_s a thin layer between a-SiO_2 and c-Si with a somewhat higher decrement δ leads to a considerable improvement in the fit shown in figure 2. The difference between the δ-values for c-Si and a-SiO_2 is so small that the periodic intensity modulation of the Kiessig interferences has a very low amplitude without the assumption of an intermediate layer. What kind of layer could this be? High-resolution transmission electron microscopy (HRTEM) images lead us to propose the existence of a c-SiO_2 layer [1, 2, 24] of hexagonal symmetry known as tridymite. The local thickness of this layer has been determined to be 7 Å. This value is not in contradiction with the parameters given in table 1 considering that the x-ray reflection measurements give the average thickness over the whole surface of the sample. Since lattice distortions are necessary

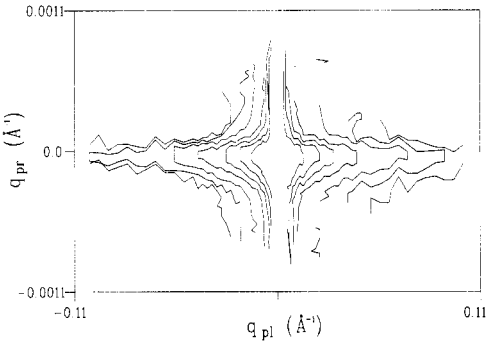

Figure 4. Isointensity contours around the (400) reflection of silicon for sample C_s. The full lines represent intensities normalized to the intensity I_0 of the (400) reflection with $I/I_0 = 2, 1, 0.5, 0.2, \ldots, 10^{-5}$. The axes are given as offset from the exact Bragg position.

for epitaxial growth of tridymite on silicon, compressing forces possibly lead to a higher density of the tridymite layer. This can effect a decrement for tridymite which is higher than the value for c-Si.

For samples A_r and A_s with thick oxide layers no such intermediate layer was found. The thickness $d_2 < 20$ Å of this additional layer is too small compared with the 1400 Å oxide layer to influence the reflection curves noticeably. Neither the roughness parameter Δz^2 nor the thickness of the transition layer from a-SiO_2 to vacuum shows any dependence on the roughening procedure chosen. Furthermore the results of the reflection measurements do not show the existence of an interface roughness or a transition layer between a-SiO_2 and c-Si. On an ångström scale all samples possess nearly the same roughness. This result is supplied by the x-ray diffraction.

The rocking curves, on the other hand, seem to be influenced by the kind of etching procedure used. All etched samples show a sizeable portion of long-range undulations of the a-SiO_2 surface.

The second type of measurement near the Si(400) reciprocal lattice point $\boldsymbol{Q}_{(400)}$ was used to obtain more exact information about the microroughness of the surface of the silicon substrate. Because the substrate crystal is perfect, the CTR can deliver this information. The experiment was aimed at obtaining intensity contours around the Si(400) reflection, or at least the direction and the intensity profile of the CTR. For this purpose the experiments were performed by varying the angle θ of the sample as a function of the scattering angle Φ. A typical result is shown in figure 4. The data have been transformed to the reciprocal space and are presented in a coordinate system with the axis parallel and perpendicular to $\boldsymbol{Q}_{(400)}$. The [011] direction is denoted as $\boldsymbol{q}_{pr}$ and the [100] direction as $\boldsymbol{q}_{pl}$.

By variation in the power of the x-ray source and of the counting time, seven orders of magnitude in the intensity can be covered for all samples, except for samples A_r and B_r (expected to be rough). The rocking curves of these samples show a mosaic spread of 0.05°. This FWHM is 25 times greater than the resolution of the diffractometer which is better than 0.002°. For these samples the dynamical range is only about four orders of magnitude and hence because of the counting statistics no CTR can be observed.

Figure 4 shows the isointensity contours for sample C_s. The lines are not continuous because the whole contour plot is composed of 101 rocking curves. The plot is constructed by connecting the equivalent points of neighbouring rocking curves. The lines represent intensities normalized to the intensity I_0 of the (400) reflection with $I/I_0 = 2, 1, 0.5, 0.2, \ldots, 10^{-5}$.

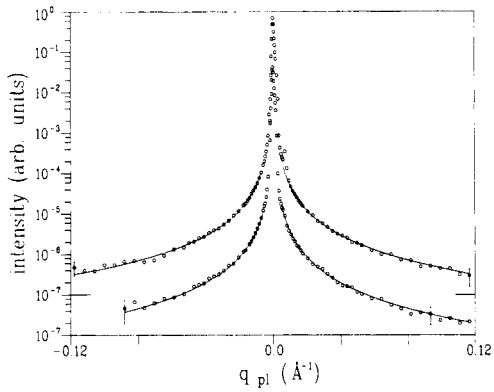

Figure 5. CTRs for sample C_r (bottom curve, ○) and sample C_s (top curve, ○) and the results of the calculation (——) with an exponent r for the intensity decay.

Table 2. Results of the fits to the intensity of the CTRs of four samples. The roughness was described by a static DWF with the roughness parameter Δz^2 and by an exponent r (see text). The χ^2-values are calculated by supposing a 5% error for each data point.

Parameter (units)	Value for the following samples			
	A_s	B_s	C_r	C_s
$\sqrt{\Delta z^2}$ (Å)	4.6 ± 0.9	1.9 ± 1.5	4.8 ± 0.7	2.2 ± 0.7
r	2.09 ± 0.04	2.04 ± 0.04	2.12 ± 0.02	2.05 ± 0.02
χ^2	1.5	0.7	0.8	0.7

The isointensity contours show that the direction of the CTR is exactly parallel to the reciprocal lattice vector $\boldsymbol{Q}_{(400)}$, i.e. in the direction of q_{pl}. The FWHM of the CTR in the direction of q_{pr} is 1.2×10^{-4} Å^{-1}. This corresponds to the resolution of the diffractometer near $|\boldsymbol{Q}| = 4.6$ Å^{-1}. The intensity extending parallel to q_{pr} near $q_{pl} = 0$ is caused by the monochromator and analyser crystal. Because these too are perfect crystals, they also give rise to a CTR. The three CTRs form a star-like intensity distribution around a reciprocal lattice point called a resolution star. The CTR of the monochromator and analyser including the angle θ_B of the Bragg position between them and the CTR of the sample. Because of the distorted scale in figure 4 these two streaks seem to be perpendicular to the CTR of the sample.

After subtraction of the background and the thermal diffuse scattering the cut parallel to q_{pl} for $q_{pr} = 0$ gives the intensity curves of the CTR shown in figure 5 for sample C_r (bottom curve) and sample C_s (top curve). The full curves represent the results of the least-squares fits considering a real exponent r (equation (9)) for the surface roughness. Additionally a model with a DWF was fitted. The results are given in table 2. For the same reason as for the reflection measurements the χ^2-values were not based on statistical errors but on a 5% error of each data point.

Both models for the surface roughness show that all four samples have almost perfect crystal surfaces. The intensity decrease of the CTR is nearly q^{-2} or, alternatively, the value for Δz^2 in the static DWF is very small. This means that the oxidation process has only a small influence on the microroughness of the silicon surface. Nor does the removal

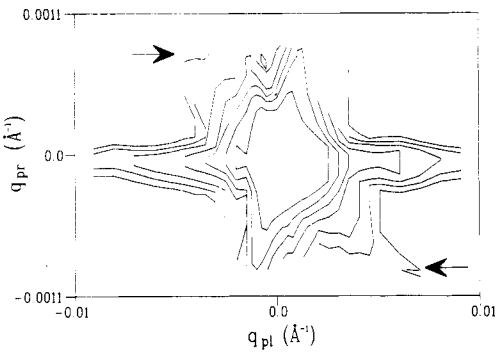

Figure 6. Isointensity contours around the (400) reflection of silicon of sample C_s for a smaller area than given in figure 4. The lines represent intensities normalized to the intensity I_0 of the (400) reflection with $I/I_0 = 2, 1, 0.5, 0.2, \ldots, 10^{-3}$. The arrows mark the additional streak, enclosing an angle of 9° with the CTR.

of the oxide layer by etching with HF solution increase the surface roughness on an ångström scale but, as we have seen, it causes undulations of the near-surface region. This leads to the small mosaic spread which gives rise to additional scattering in the direction of q_{pr}. These results are equivalent to those found by HRTEM images by several groups [1, 2, 25, 26] and x-ray diffraction studies on a-SiO_2/c-Si(111) [5, 27]. Apart from long-range undulations on the silicon surface these workers find a roughness of 2 Å in a gaussian description. A small increase in surface roughness is reached by etching with 5% HCl [26]. HF solution is much more corrosive than HCl solution and thus a stronger effect was expected. Therefore samples A_r and B_r show a strongly increased roughness of the silicon surface compared with samples A_s and B_s, as indicated by their broad rocking curves. Equally sample C_r shows a higher interface roughness than sample C_s but the rocking curves are narrower than those of samples A_r and B_r and a CTR can be studied to evaluate a roughness parameter.

A further result of the measurement of the isointensity contours cannot be recognized in figure 4. Therefore figure 6 shows a smaller region around the reciprocal lattice point (400). Besides the CTR and the streaks near $q_{pl} = 0$ caused by the monochromator and analyser crystal a further streak (marked by arrows) can be seen. It has no symmetrical equivalent. This streak shows an intensity maximum at a distance of $q_{pl} = 8.1 \times 10^{-3}$ Å^{-1} and $q_{pr} = -1.15 \times 10^{-3}$ Å^{-1} from the Si(400) reflection. The streak has an angle of 9° to the normal of the silicon surface. The FWHM of the rocking curve across this maximum is three times larger than that of the Si(400) reflection and the intensity is four orders of magnitude smaller. This additional scattering intensity was found for all four samples where a CTR could be seen. Because it forms a small Bragg reflection, the scattering could be due to a crystalline region on the silicon surface having a nearly epitaxial lattice. This could be the c-SiO_2 layer of tridymite mentioned above. Lattice distortions allow epitaxial growth of tridymite on silicon. The lattice mismatch along the [100] direction could be due to the small discrepancy between the two observed Bragg reflections. A further mismatch along the [011] direction can cause a tilt of the reflection planes, resulting in an angle of 9° between the CTR from silicon and the other streak.

By comparing the intensities of the two reflections, one can estimate a thickness of 5 Å for the crystalline layer which is in good agreement with the value found by HRTEM images [1, 2]. This is nearly the same order of magnitude for the thickness of the intermediate layer found by the reflection measurements described above.

The results of the reflection measurements and the isointensity contours around the (400) reciprocal lattice point of silicon cannot prove that the intermediate layer consists of tridymite but they give additional evidence to that of the HRTEM images.

Further Bragg reflections of the tridymite layer could not be found because the TCD is not suitable for such a search in the reciprocal space. Owing to the high resolution of the diffractometer, only a small volume element of the reciprocal space can be seen during one measurement. Therefore unacceptably long measurement times would be necessary to search for further tridymite Bragg reflections if really visible.

5. Conclusion

With a high-resolution TCD both the reflectivity close to the total external reflection and the intensity distribution around the (400) reflection of several samples of a-SiO_2/c-Si(100) were studied. The thicknesses of the a-SiO_2 layers, their optical constants for x-ray radiation and their surface and interface roughnesses on an ångström scale were evaluated by the reflectivity measurements using Parratt's approach. Although one part of each pair of samples was etched and oxidized over several cycles, no increase in the microroughness of the surface was observed. For the samples with a thin oxide layer the reflectivity hints that an intermediate layer between a-SiO_2 and c-Si(100) exists with a slightly higher electron density and a thickness of about 20 Å.

A more exact statement about the surface roughness of c-Si(100) was reached by measuring the crystal truncation rod near the (400) reflection. The results showed that, for all samples which were not etched, the intensity decreased almost as expected for a sharp surface of a perfect crystal. Most of the etched samples showed a pronounced mosaic spread, reducing the dynamical range. This prevents the observation of a CTR. Furthermore the isointensity contours around the (400) reflection show an intensity streak crossing the silicon reflection which is not a part of the resolution star. This streak, forming an angle of 9° with the CTR, has an intensity maximum very close to the silicon peak. By comparing the intensity ratio a thickness of 5 Å for the corresponding crystalline layer was estimated. This layer could be composed of tridymite, a crystalline form of SiO_2, epitaxially grown on the Si(100) surface with some lattice distortions.

Acknowledgments

The authors thank E Pehlke for some helpful discussions and calculations in connection with the reflectivity measurements. The experiments were supported by the Bundesministerium für Forschung und Technologie under contract 05401ABI2.

References

[1] Ourmazd A, Taylor D W and Rentschler J A 1987 *Phys. Rev. Lett.* **59** 213
[2] Ourmazd A and Bevk J 1988 *Materials Research Society Symposium 105* (Pittsburgh, PA: Materials Research Society) p 1
[3] Himpsel F J, McFeely F R, Taleb-Ibrahimi A and Yarmoff J A 1988 *Phys. Rev.* B **38** 6084
[4] Fuoss P H, Norton L J, Brennan S and Fischer-Colbrie A 1988 *Phys. Rev. Lett.* **60** 600
[5] Cowley R A and Ryan T W 1987 *J. Phys. D: Appl. Phys.* **20** 61
[6] Parratt L G 1954 *Phys. Rev.* **95** 359
[7] Névot L and Croce P 1980 *Rev. Phys. Appl.* **15** 761
[8] Wu E S and Webb W W 1973 *Phys. Rev.* A **8** 2065
[9] Robinson I K 1986 *Phys. Rev.* B **33** 3830

[10] Bloch R, Brügemann L and Press W 1989 *J. Phys. D: Appl. Phys.* **22** 1136
[11] Cowley R A 1987 *Acta Crystallogr.* A **43** 825
[12] Brügemann L 1989 *PhD Thesis* University of Kiel
[13] Andrews S R and Cowley R A 1985 *J. Phys. C: Solid State Phys.* **18** 6427
[14] Eisenberger P, Alexandropoulos N G and Platzman P M 1972 *Phys. Rev. Lett.* **28** 1519
[15] Beckman P and Spizzichino A 1963 *The Scattering of EM Waves from Rough Surfaces* (Oxford: Pergamon)
[16] Andreev A V, Michette A G and Renwick A 1988 *J. Mod. Opt.* **35** 1667
[17] Pehlke E 1989 private communications
[18] Darwin C G 1914 *Phil. Mag.* **27** 315, 615
[19] Zachariasen W H 1945 *Theory of X-ray Diffraction in Crystals* (New York: Wiley)
[20] Bale H D and Schmidt P W 1984 *Phys. Rev. Lett.* **53** 596
[21] Kiessig H 1931 *Ann. Phys.* **10** 715
[22] Croce P and Névot L 1976 *Rev. Phys. Appl.* **11** 113
[23] Weast R C (ed) 1985–6 *Handbook of Chemistry and Physics* (West Palm Beach, FL: CRC Press) p B138
[24] Rochet F, Rigo S, Froment M, D'Anterroches C, Maillot C, Roulet H and Dufour G 1986 *Adv. Phys.* **35** 237
[25] Krivanek O L and Mazur J H 1980 *Appl. Phys. Lett.* **37** 392
[26] Goodnick S M, Ferry D K, Wilmsen C W, Liliental Z, Fathy D and Krivanek O L 1985 *Phys. Rev.* B **32** 8171
[27] Afanasév A M, Aleksandrov P A, Fanchenko S S, Chaplanov V A and Yakimov S S 1986 *Acta Crystallogr.* A **42** 116